https://doi.org/10.20965/jaciii.2019.p0997

Paper:

Joint Trajectory Planning Based on Minimum Euclidean Distance of Joint Angles of a Seven-Degrees-of-Freedom Manipulator for a Sequential Reaching Task

Yoshiaki Taniai and Tomohide Naniwa

Graduate School of Engineering, University of Fukui
3-9-1 Bunkyo, Fukui, Fukui 910-8507, Japan
E-mail: taniai@u-fukui.ac.jp

[Received October 30, 2017; accepted June 25, 2019]

When a nuclear power disaster occurs at a nuclear power plant, it is hazardous for humans to enter the plant. If robots could remove radioactive substances adhering to a plane such as a plant wall, humans would be able to enter the plant to investigate the situation and to work. In this study, to efficiently remove radioactive substances from a wall with a manipulator, we examined joint trajectory planning based on the minimum Euclidean distance of joint angles of a seven-degrees-of-freedom (7-DOF) serial link manipulator for a sequential reaching task on a plane. We demonstrate the planning for the sequential reaching task, which is an iterative point-to-point reaching movement between positions on a plane. The joint angles for each target position were obtained based on the inverse kinematics for an arm angle, and the optimal arm angles within the constraints of the joint angles were computed by the sequential quadratic programming method. The optimal trajectories for the arm angles were compared with the trajectories of the joint angles that were the eight inverse kinematic solutions for a fixed arm angle. The result showed that through optimal planning, an efficient trajectory within the movable ranges of the joint angles could be obtained for the sequential reaching task.

Keywords: optimal planning, sequential reaching task, 7-DOF manipulator, minimum Euclidean distance, movable ranges

1. Introduction

When a nuclear disaster occurs at a nuclear power plant, the radiation dose inside the nuclear power plant is high. It is then hazardous for humans to enter the plant. If robots could remove radioactive substances adhering to a plane such as a plant wall, humans would be able to enter the nuclear power plant and investigate the situation or work.

Radioactivity can be decontaminated using a device that blows high-pressure water or abrasives, or irradiates a laser onto a surface such as a wall. The device is attached to an end effector of a manipulator and can remove radioactive substances from various places when the manipulator is moved [1–3]. The laser decontamination device and the manipulator are generally mounted on a mobile robot with wheels or crawlers. A laser decontamination device that measures the distance to the surface and simultaneously removes radioactive material can decontaminate a non-uniform or non-smooth surface [3]. The plane of a wall can be obtained by the Hough transformation or by random sample consensus from point cloud data, which can be obtained by a 3D laser scanner.

Although manipulators with redundancy are excellent for singularity avoidance, collision avoidance, and maintaining high manipulability, there are infinite combinations of joint angles that realize the position and orientation of the end effector; the inverse kinematic solution of the manipulator cannot be uniquely determined [4]. Bicriteria velocity minimization based on a primal-dual neural network has been proposed to resolve the redundancy problem for robot manipulators [5]. The study demonstrated the tasks of circular path tracking and straight path tracking considering the limitations of the angles and angular velocities of a manipulator (PUMA560). On the other hand, solutions to the inverse kinematics of a seven-degrees-of-freedom (7-DOF) serial link manipulator using the arm angle have been proposed [6]. The arm angle is the angle between the arm plane and a reference plane, and it is a scalar variable by which the redundancy of the 7-DOF manipulator is parameterized to determine the joint angles for a given end effector position and orientation [4]. When the arm angle of the manipulator is given, there are eight solutions according to inverse kinematics. If we can determine the optimal trajectory of arm angles that suppress the change in joint angles of the manipulator within the movable ranges of the joint angles, it would be possible to remove the radioactive substances efficiently.

In this study, we examine joint trajectory planning based on the minimum Euclidean distance of joint angles of a 7-DOF serial link manipulator for a sequential reaching task in a plane. We demonstrate the planning for a sequential reaching task, which is an iterative

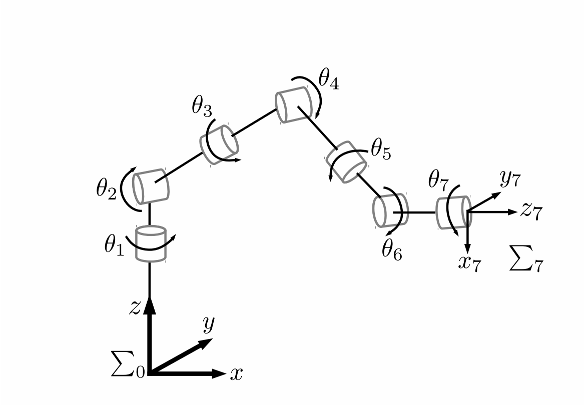

Fig. 1. 7-DOF serial link manipulator.

point-to-point reaching movement between positions on a plane. The joint angles for the target position are obtained based on the inverse kinematics for the arm angle, and the optimal arm angles with the constraints of the joint angles are computed by the sequential quadratic programming method. The optimal trajectories of the joint angles are then compared with the trajectories of the joint angles that are the eight inverse kinematic solutions for a fixed arm angle. This paper is organized as follows. Section 2 describes the kinematics of the 7-DOF manipulator, the task, the inverse kinematic solutions, and the optimal planning based on the minimum Euclidean distance. Section 3 presents the results of both the optimal planning and the inverse kinematics. Finally, Section 4 concludes the paper.

2. Method

We computed optimal trajectories based on the minimum Euclidean distance of the joint angles of a 7-DOF serial link manipulator within the movable ranges of the manipulator joints for a sequential reaching task. The optimal trajectories of the joint angles were compared with the trajectories of the joint angles that were the eight inverse kinematic solutions for a fixed arm angle.

2.1. Kinematics of the 7-DOF Manipulator

We used a Spherical-Revolute-Spherical type manipulator as the 7-DOF serial link manipulator (**Fig. 1**). The shoulder joint is a spherical joint consisting of θ_1, θ_2, and θ_3, the elbow joint is a revolute joint consisting of θ_4, and the wrist joint is a spherical joint consisting of θ_5, θ_6, and θ_7. The coordinate system of joints $\Sigma_i (i = 1,2,\dots,7)$ is fixed to each joint θ_i. The base coordinate system Σ_0 is fixed to the root of the manipulator, and the coordinate system Σ_7 is set at the endpoint of the manipulator. **Tables 1** and **2** show the link parameters based on the Denavit–Hartenberg rules [7] and the movable ranges of the joint angles for the 7-DOF serial link manipulator (SIA-20, Yaskawa Electric Corporation).

The position ${}^0\boldsymbol{x}_7$ and orientation ${}^0\boldsymbol{R}_7$ of the end effector

Table 1. Link parameters for SIA-20.

i	a_i [m]	α_i [rad]	d_i [m]	θ_i [rad]
1	0	$-\pi/2$	0.36	θ_1
2	0	$\pi/2$	0	θ_2
3	0	$-\pi/2$	0.42	θ_3
4	0	$\pi/2$	0	θ_4
5	0	$-\pi/2$	0.40	θ_5
6	0	$\pi/2$	0	θ_6
7	0	0	0.111	θ_7

Table 2. Movable ranges of joint angles for SIA-20.

i	θ_i^{min} [°]	θ_i^{max} [°]
1	−180	180
2	−110	110
3	−170	170
4	−130	130
5	−180	180
6	−110	110
7	−180	180

are expressed as follows [6]:

$$ {}^0\boldsymbol{x}_7 = {}^0\boldsymbol{l}_{bs} + {}^0\boldsymbol{R}_\Theta {}^0\boldsymbol{R}_3^o \left\{ {}^3\boldsymbol{l}_{se} + {}^3\boldsymbol{R}_4 \left({}^4\boldsymbol{l}_{ew} + {}^4\boldsymbol{R}_7 {}^7\boldsymbol{l}_{wt} \right) \right\} \quad (1) $$

$$ {}^0\boldsymbol{R}_7 = {}^0\boldsymbol{R}_\Theta {}^0\boldsymbol{R}_3^o {}^3\boldsymbol{R}_4 {}^4\boldsymbol{R}_7 \quad \dots\dots\dots\dots \quad (2) $$

where ${}^i\boldsymbol{R}_j$ is the rotation from the coordination Σ_j to the coordination Σ_i, ${}^0\boldsymbol{R}_\Theta$ is the rotation of the arm angle Θ, which is the rotation around the axis connecting the shoulder joint and the wrist joint, and ${}^i\boldsymbol{R}_j^o$ is the rotation when the arm plane corresponds to the reference plane (i.e., $\Theta = 0$), ${}^0\boldsymbol{l}_{bs} = [0,0,d_1]^T$, ${}^3\boldsymbol{l}_{se} = [0,-d_3,0]^T$, ${}^4\boldsymbol{l}_{ew} = [0,0,d_5]^T$, and ${}^7\boldsymbol{l}_{wt} = [0,0,d_7]^T$. The rotation between coordinate systems Σ_{i-1} and Σ_i is given by

$$ {}^{i-1}R_i = \begin{bmatrix} \cos\theta_i & -\sin\theta_i \cos\alpha_i & \sin\theta_i \sin\alpha_i \\ \sin\theta_i & \cos\theta_i \cos\alpha_i & -\cos\theta_i \sin\alpha_i \\ 0 & \sin\alpha_i & \cos\alpha_i \end{bmatrix}. \quad (3) $$

The rotation ${}^0\boldsymbol{R}_\Theta$ of the arm angle is given by

$$ {}^0\boldsymbol{R}_\Theta = \boldsymbol{I}_3 + \sin\Theta \left[{}^0\boldsymbol{u}_{sw} \times \right] + (1 - \cos\Theta) \left[{}^0\boldsymbol{u}_{sw} \times \right]^2 \quad (4) $$

where $\boldsymbol{I}_3$ is the identity matrix, ${}^0\boldsymbol{u}_{sw}$ is the unit vector of ${}^0\boldsymbol{x}_{sw}$, and $\left[{}^0\boldsymbol{u}_{sw} \times \right]$ is the skew-symmetric matrix corresponding the cross product with the vector ${}^0\boldsymbol{u}_{sw}$. The vector ${}^0\boldsymbol{x}_{sw}$ from the shoulder joint to the wrist joint is expressed as follows:

$$ {}^0\boldsymbol{x}_{sw} = {}^0\boldsymbol{x}_7 - {}^0\boldsymbol{l}_{bs} - {}^0\boldsymbol{R}_7 {}^7\boldsymbol{l}_{wt}. \quad \dots\dots\dots \quad (5) $$

2.2. Task

Figure 2 shows a sequential reaching task for target points on a target plane. In the demonstration, the target plane was assumed to be on the xz-plane at $y = 0.6$ m. The ranges of the x and z positions on the plane were $-0.4 \le x \le 0.4$ and $0.2 \le z \le 1.0$, respectively. The target points $\boldsymbol{x}_d^k = (x_d^k, y_d^k, z_d^k)(k = 1,2,\dots,N)$ are evenly spaced because the laser decontaminator that is attached to the end effector emits a laser that covers approximately 100

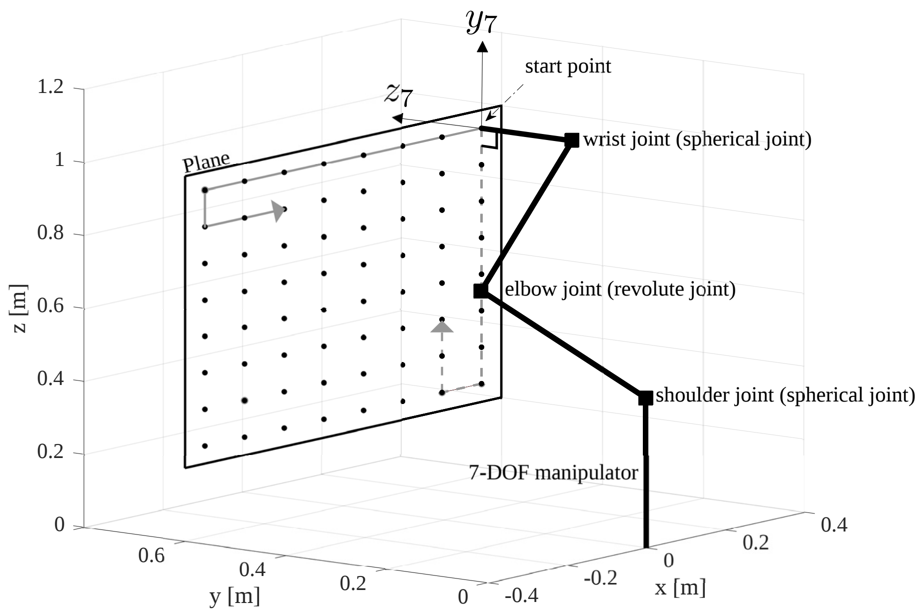

Fig. 2. Sequential reaching task on a plane. The circle points show the target points. The gray solid and dashed lines show routes based on the horizontal direction and the vertical direction, respectively. The squares show the Spherical-Revolute-Spherical joints of the 7-DOF serial link manipulator.

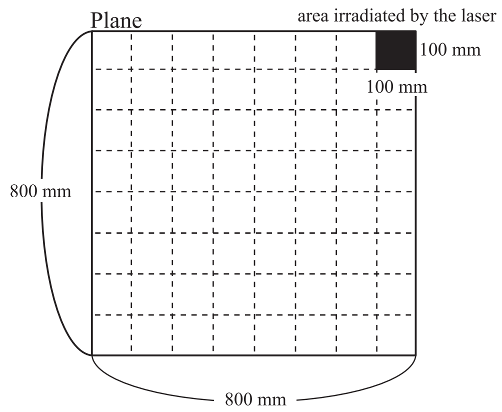

Fig. 3. Areas irradiated by the laser in a target plane. The filled area shows the area that the laser can irradiate at one time.

$\times$ 100 mm^2 (**Fig. 3**). Then, the target points of the end effector were $(x,y,z) = (-0.35+0.1\times m, 0.6, 0.25+0.1\times n)(m,n = 0,1,\ldots,7)$, and the number of target points N was 64 points in 8 rows and 8 columns. The starting point for the task was set at $(0.35, 0.6, 0.95)$. The routes of the sequential reaching motion were based on vertical and horizontal directions (**Fig. 2**). To irradiate the whole of each target area on the plane, the z-axis of the end effector has to be perpendicular to the plane, and the posture of the end effector has to remain unchanged. We assumed that the y-axis of the end effector was oriented in the direction of the z-axis of $\sum_0$. Then, the orientation of the end effector was as follows:

$$^0\boldsymbol{R}_7^d = \begin{bmatrix} -1 & 0 & 0 \\ 0 & 0 & 1 \\ 0 & 1 & 0 \end{bmatrix} \quad \ldots\ldots\ldots\ldots \quad (6)$$

2.3. Inverse Kinematics of the 7-DOF Manipulator

We followed the method of inverse kinematics for the 7-DOF manipulator proposed in [6]. If an arm angle is given, there are eight inverse kinematic solutions for the 7-DOF manipulator. Thus, the solutions by inverse kinematics are expressed as follows:

$$\theta_1 = \arctan 2(-a_{s22}\sin\Theta - b_{s22}\cos\Theta - c_{s22},\ -a_{s12}\sin\Theta - b_{s12}\cos\Theta - c_{s12}) \quad \ldots\ldots \quad (7)$$

$$\theta_2 = \arctan 2\left(\sqrt{\sum_{i=1}^{2}(a_{si2}\sin\Theta + b_{si2}\cos\Theta + c_{si2})^2},\ -a_{s32}\sin\Theta - b_{s32}\cos\Theta - c_{s32}\right) \quad \ldots\ldots \quad (8)$$

$$\theta_3 = \arctan 2(a_{s33}\sin\Theta + b_{s33}\cos\Theta + c_{s33},\ -a_{s31}\sin\Theta - b_{s31}\cos\Theta - c_{s31}) \quad \ldots\ldots \quad (9)$$

$$\theta_4 = \gamma_1 \arccos\left(\frac{\|{}^0\boldsymbol{x}_{sw}\|^2 - d_3^2 - d_5^2}{2d_3d_5}\right) \quad \ldots\ldots \quad (10)$$

$$\theta_5 = \arctan 2(\gamma_3(a_{w23}\sin\Theta + b_{w23}\cos\Theta + c_{w23}),\ \gamma_3(a_{w13}\sin\Theta + b_{w13}\cos\Theta + c_{w13})) \quad \ldots\ldots \quad (11)$$

$$\theta_6 = \gamma_3 \arctan 2\left(\sqrt{\sum_{i=1}^{2}(a_{wi3}\sin\Theta + b_{wi3}\cos\Theta + c_{wi3})^2},\ a_{w33}\sin\Theta + b_{w33}\cos\Theta + c_{w33}\right) \quad \ldots\ldots \quad (12)$$

$$\theta_7 = \arctan 2(\gamma_3(a_{w32}\sin\Theta + b_{w32}\cos\Theta + c_{w32}),\ \gamma_3(-a_{w31}\sin\Theta - b_{w31}\cos\Theta - c_{w31})) \quad \ldots \quad (13)$$

where γ_1 and γ_3 are parameters that indicate the different inverse kinematic solutions, and a_{sij}, b_{sij}, c_{sij}, a_{wij}, b_{wij}, and c_{wij} are the (i,j) elements of the matrices $\boldsymbol{A}_s$, $\boldsymbol{B}_s$, $\boldsymbol{C}_s$,

Table 3. Combinations of parameters for the different inverse kinematic solutions.

Solution No.	γ_1	γ_2	γ_3
1	$+1$	$+1$	$+1$
2	$+1$	$+1$	-1
3	$+1$	-1	$+1$
4	$+1$	-1	-1
5	-1	$+1$	$+1$
6	-1	$+1$	-1
7	-1	-1	$+1$
8	-1	-1	-1

$\boldsymbol{A}_w$, $\boldsymbol{B}_w$, and $\boldsymbol{C}_w$, respectively;

$$\boldsymbol{A}_s = \left[{}^0\boldsymbol{u}_{sw}\times\right]\,{}^0\boldsymbol{R}_3^o \qquad (14)$$

$$\boldsymbol{B}_s = -\left[{}^0\boldsymbol{u}_{sw}\times\right]^2\,{}^0\boldsymbol{R}_3^o \qquad (15)$$

$$\boldsymbol{C}_s = \left[{}^0\boldsymbol{u}_{sw}{}^0\boldsymbol{u}_{sw}^T\right]\,{}^0\boldsymbol{R}_3^o \qquad (16)$$

$$\boldsymbol{A}_w = {}^3\boldsymbol{R}_4^T\,\boldsymbol{A}_s^T\,{}^0\boldsymbol{R}_7^d \qquad (17)$$

$$\boldsymbol{B}_w = {}^3\boldsymbol{R}_4^T\,\boldsymbol{B}_s^T\,{}^0\boldsymbol{R}_7^d \qquad (18)$$

$$\boldsymbol{C}_w = {}^3\boldsymbol{R}_4^T\,\boldsymbol{C}_s^T\,{}^0\boldsymbol{R}_7^d. \qquad (19)$$

The joint angles θ_1°, θ_2°, θ_3° when the arm plane corresponds to the reference plane are as follows:

$$\theta_1^\circ = \arctan 2(x_{sw1}, -x_{sw2}) - \arctan 2\left(\gamma_2\sqrt{x_{sw1}^2 + x_{sw2}^2}, 0\right) \qquad (20)$$

$$\theta_2^\circ = \arctan 2(b_1, b_2) - \arctan 2\left(\gamma_2\sqrt{b_1^2 + b_2^2 - x_{sw3}^2}, -x_{sw3}\right) \qquad (21)$$

$$\theta_3^\circ = 0 \qquad (22)$$

where ${}^0\boldsymbol{x}_{sw} = [x_{sw1}, x_{sw2}, x_{sw3}]^T$, $b_1 = d_5 \sin\theta_4$, $b_2 = -d_3 - d_5\cos\theta_4$, and γ_2 is a parameter that indicates the different inverse kinematic solutions. The different inverse kinematic solutions are represented by the combinations of $\gamma_1 = \pm 1$, $\gamma_2 = \pm 1$, and $\gamma_3 = \pm 1$ (**Table 3**).

2.4. Constrained Optimization Problem

We computed the optimal trajectories of arm angles $\boldsymbol{\Theta}$ for each inverse kinematic solution (eight solutions), and then obtained the optimal trajectories of the joint angles from the trajectories of the arm angles. The evaluation function based on the minimum Euclidean distance of the joint angles takes the following form:

$$E(\boldsymbol{\Theta}) = \sum_{k=1}^{N-1}\left\|\boldsymbol{\theta}^{k+1} - \boldsymbol{\theta}^k\right\| \qquad (23)$$

where $\boldsymbol{\Theta} = [\Theta^1, \Theta^2, \ldots, \Theta^k, \ldots, \Theta^N]^T$, k indicates the index of the target point, $\|\boldsymbol{x}\|$ denotes the Euclidean norm of $\boldsymbol{x}$, and $\boldsymbol{\theta}^k = [\theta_1^k, \theta_2^k, \ldots, \theta_7^k]^T$. The inequality constraints of the optimization problem are as follows:

$$-\pi \leq \Theta^k \leq \pi \qquad (24)$$

$$\theta_i^{min} \leq \theta_i^k \leq \theta_i^{max} \qquad (25)$$

where θ^{min} and θ^{max} show the lower bound and upper bound of each joint angle, respectively. Eqs. (24) and (25) show the constraints for the arm angle and the movable ranges of the joint angles, respectively. Note that because the joint angle θ_4 is not dependent on the arm angle (Eq. (10)), the constraint of the joint angle θ_4^k cannot be included in the constrained optimization problem (Eq. (25)). When θ_4^k does not satisfy the movable range of the joint angle, there is no inverse kinematic solution.

The initial values of the arm angles $\boldsymbol{\Theta}$ were all set to $\pi/4$ rad. The optimal arm angles were computed by the sequential quadratic programming method. The method was executed using SNOPT (Stanford Business Software, Inc.) [8].

3. Result

Tables 4 and **5** show the Euclidean distances and constraints of the inverse kinematic solutions for the horizontal route and the vertical route, respectively. The inverse kinematic solutions were obtained when the arm angles at the target points were set to $\pi/4$. Half of the solutions did not satisfy the constraints. Although in the horizontal route the eighth solution satisfied the constraints and covered the smallest Euclidean distance ($E = 39.369$ rad), the third solution in the vertical route covered a smaller Euclidean distance ($E = 34.660$ rad).

Tables 6 and **7** show the Euclidean distances and constraints of the optimal solutions based on the minimum Euclidean distance of the joint angles for the horizontal route and the vertical route, respectively. As the result of the constrained optimization, all optimal solutions satisfied the constraints of the joint angles. Furthermore, the sixth optimal solution along the horizontal route covered the smallest Euclidean distance ($E = 18.246$ rad) and was smaller than the inverse kinematic solutions. Note that although the constraints were satisfied, there were also cases where the Euclidean distance was large. By selecting the optimal solution with the smallest Euclidean distance among the eight solutions, it was possible to obtain the optimal angles for efficiently removing radioactive substances.

Figure 4 shows the trajectories of the joint angles of solution No.6 along the horizontal route. In the inverse kinematic solution, θ_2 did not satisfy the constraint, but the optimal solution satisfied the constraint. Furthermore, the change at each joint angle of the optimal solution was smaller than that of inverse kinematics; that is, the Euclidean distance of the optimal solution was smaller than that of inverse kinematics. **Fig. 5** shows the trajectories of the joint angles of solution No.7 along the horizontal route. Although the constraints were satisfied, the change in each joint angle of the optimal solution was larger than that of inverse kinematics; that is, the Euclidean distance of the optimal solution was larger than that of inverse kinematics. Because the optimized result was not always right, it would be necessary to select the best solution out of the eight optimal solutions.

Table 4. Euclidean distances and constraints of the inverse kinematic solutions for the horizontal route.

Solution No.	Value [rad]	Constraints
1	73.489	○
2	64.610	○
3	43.017	○
4	67.554	×
5	21.358	×
6	21.358	×
7	67.554	×
8	39.369	○

Table 5. Euclidean distances and constraints of the inverse kinematic solutions for the vertical route.

Solution No.	Value [rad]	Constraints
1	62.225	○
2	88.833	○
3	34.660	○
4	48.941	×
5	19.926	×
6	19.926	×
7	48.941	×
8	64.988	○

Table 6. Euclidean distances and constraints of the optimal solutions for the horizontal route.

Solution No.	Value [rad]	Constraints
1	64.097	○
2	70.586	○
3	22.524	○
4	72.602	○
5	47.618	○
6	18.246	○
7	187.105	○
8	28.681	○

Table 7. Euclidean distances and constraints of the optimal solutions for the vertical route.

Solution No.	Value [rad]	Constraints
1	67.451	○
2	79.829	○
3	20.749	○
4	74.308	○
5	58.750	○
6	20.749	○
7	64.192	○
8	51.485	○

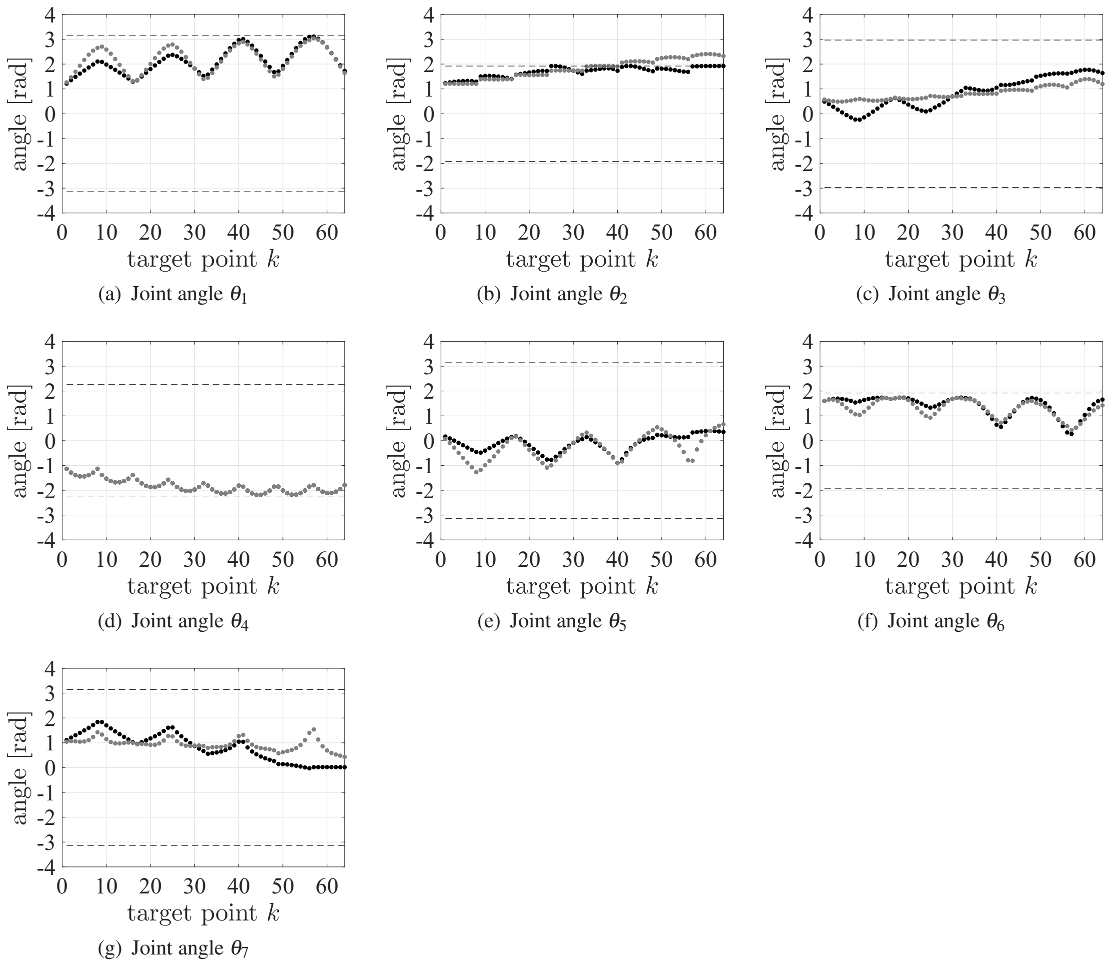

Fig. 4. Trajectories of joint angles of solution No.6 along the horizontal route. The black and gray dotted lines show the optimal solution based on the minimum Euclidean distance and the inverse kinematic solution, respectively. The dashed lines show the lower bounds and the upper bounds of the joint angles. Note that the fourth joint angle is the same in the inverse kinematic solution and the optimal solution because the joint angle is independent of the arm angle.

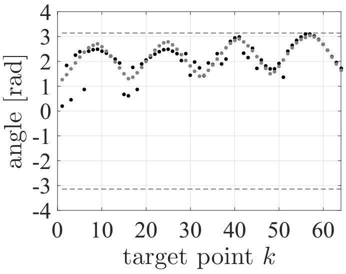

(a) Joint angle θ_1

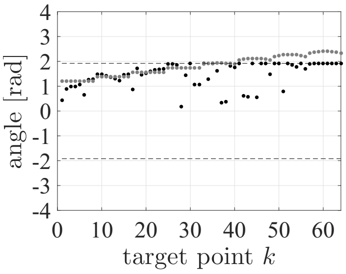

(b) Joint angle θ_2

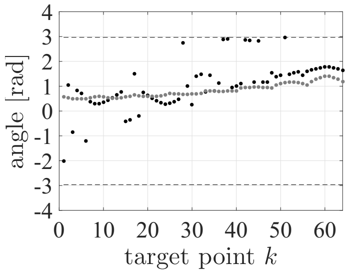

(c) Joint angle θ_3

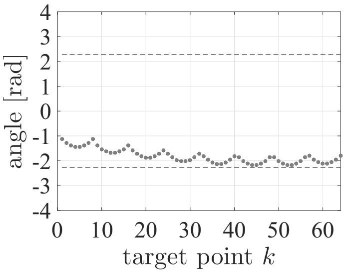

(d) Joint angle θ_4

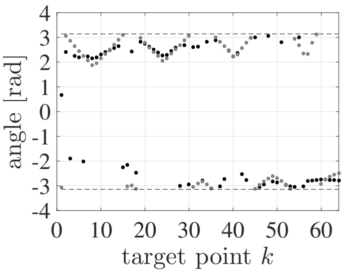

(e) Joint angle θ_5

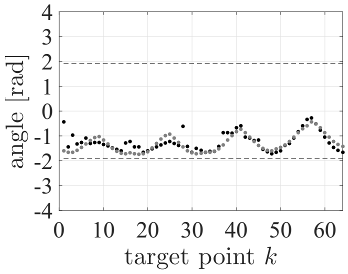

(f) Joint angle θ_6

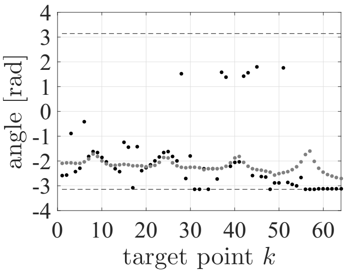

(g) Joint angle θ_7

Fig. 5. Trajectories of joint angles of solution No.7 along the horizontal route. The black and gray dotted lines show the optimal solution based on the minimum Euclidean distance and the inverse kinematic solution, respectively. The dashed lines show the lower bounds and the upper bounds of the joint angles. Note that the fourth joint angle is the same in the inverse kinematic solution and the optimal solution because the joint angle is independent of the arm angle.

4. Conclusion

We proposed optimal trajectory planning based on the minimum Euclidean distance of joint angles of a 7-DOF serial link manipulator within the movable ranges of the manipulator joints for a sequential reaching task. As the result of the optimal planning, the optimal solution covered the smallest Euclidean distance and satisfied the movable ranges of the joint angles. From the result, the optimal planning obtained an efficient trajectory for the joint angles of the 7-DOF serial link manipulator for the sequential reaching task. Furthermore, because the optimizations for the different inverse kinematic solutions are irrelevant, the optimal solution could be efficiently obtained by parallel processing such as with OpenMP. In future work, in the case where a wall is quite uneven and not smooth, or when multiple planes are included, it will also be necessary to consider the constraint that the manipulator does not contact the wall.

References:

[1] S. Kawatsuma, “Robots for Nuclear Emergency in Germany and France,” J. of the Robotics Society of Japan, Vol.32, No.1, pp. 25-31, 2014 (in Japanese).

[2] L. Morikawa, T. Hashimoto, N. Shimonabe, M. Yano, H. Onitsuka, and J. Fujita, “Development of the Remote Decontamination Robot “MHI-MEISTeR II” for an Upper Floor of Reactor Building in Fukushima Daiichi NPP,” E-J. of Advanced Maintenance, Vol.9, No.2, pp. 126-131, 2017.

[3] E. J. Minehara, “Laser decontamination device,” US Patent No.US9174304B2, 2015.

[4] K. Kreutz-Delgado, M. Long, and H. Seraji, “Kinematic Analysis of 7-DOF Manipulators,” Int. J. of Robotics Research, Vol.11, No.5, pp. 469-481, 1992.

[5] Y. Zhang, B. Cai, L. Zhang, and K. Li, “Bi-criteria Velocity Minimization of Robot Manipulators Using a Linear Variational Inequalities-Based Primal-Dual Neural Network and PUMA560 Example,” Advanced Robotics, Vol.22, No.13-14, pp. 1479-1496, 2008.

[6] M. Shimizu, H. Kakuya, W.-K. Yoon, K. Kitagaki, and K. Kosuge, “Analytical Inverse Kinematic Computation for 7-DOF Redundant Manipulators With Joint Limits and Its Application to Redundancy Resolution,” IEEE Trans. on Robotics, Vol.24, No.5, pp. 1131-1142, 2008.

[7] H. Asada and J.-J. E. Slotine, “Robot Analysis and Control,” John Wiley & Sons, 1986.

[8] P. E. Gill, W. Murray, and M. A. Saunders, “SNOPT: An SQP Algorithm for Large-Scale Constrained Optimization,” SIAM Review, Vol.47, No.1, pp. 99-131, 2005.

Name:
Yoshiaki Taniai

Affiliation:
Senior Assistant Professor, Human and Artificial Intelligent System, Graduate School of Engineering, University of Fukui

Address:
3-9-1 Bunkyo, Fukui, Fukui 910-8507, Japan

Brief Biographical History:
2011- Assistant Professor, University of Fukui
2016- Senior Assistant Professor, University of Fukui

Main Works:
- "Evaluation of Trajectory Planning Models for Arm-Reaching Movements Based on Energy Cost," Neural Computation, Vol.21, No.9, pp. 2634-2647, 2009.
- "Optimality of Upper-Arm Reaching Trajectories Based on the Expected Value of the Metabolic Energy Cost," Neural Computation, Vol.27, No.8, pp. 1721-1737, 2015.

Membership in Academic Societies:
- The Institute of Electronics, Information and Communication Engineers (IEICE)
- The Robotics Society of Japan (RSJ)

Name:
Tomohide Naniwa

Affiliation:
Professor, Human and Artificial Intelligent Systems, Graduate School of Engineering, University of Fukui

Address:
3-9-1 Bunkyo, Fukui, Fukui 910-8507, Japan

Brief Biographical History:
1990- Assistant Professor, The University of Tokyo
1995- Lecturer, Yamaguchi University
1998- Associate Professor, Yamaguchi University
2000- Associate Professor, University of Fukui
2007- Full Professor, University of Fukui

Main Works:
- "An Adaptive Controller Dominant-Type Hybrid Adaptive and Learning Controller for Trajectory Tracking of Robot Manipulators," Advanced Robotics, Vol.26, No.1-2, pp. 45-61, 2012.

Membership in Academic Societies:
- The Institute of Electrical and Electronic Engineers (IEEE)
- The Robotics Society of Japan (RSJ)
- The Society of Instrument and Control Engineers (SICE)
- The Japan Society of Mechanical Engineers (JSME)